Title

Epitope-specific affinity maturation improved stability of potent protease inhibitory antibodies

Journal

Biotechnology and Bioengineering, 115(11)

ISSN

0006-3592

Authors

Lopez, Tyler
Chuan, Chen
Ramirez, Aaron
et al.

Publication Date

2018-11-01

DOI

10.1002/bit.26814

Peer reviewed

HHS Public Access

Author manuscript

Biotechnol Bioeng. Author manuscript; available in PMC 2019 November 01.

Published in final edited form as:

Biotechnol Bioeng. 2018 November ; 115(11): 2673–2682. doi:10.1002/bit.26814.

Epitope Specific Affinity Maturation Improved Stability of Potent Protease Inhibitory Antibodies

Tyler Lopez[1], **Chen Chuan**[1], **Aaron Ramirez**[1], **Kuan-Hui E. Chen**[2], **Mary Y. Lorenson**[2], **Chris Benitez**[1], **Zahid Mustafa**[1], **Henry Pham**[1], **Ramon Sanchez**[1], **Ameae M. Walker**[2], and **Xin Ge**[1,*]

[1]Department of Chemical and Environmental Engineering, Bourns College of Engineering,

[2]Division of Biomedical Sciences, School of Medicine, University of California Riverside.

Abstract

Targeting effectual epitopes is essential for therapeutic antibodies to accomplish their desired biological functions. This study developed a competitive dual color FACS to maturate a matrix-metalloprotease 14 (MMP-14) inhibitory antibody. Epitope specific screening was achieved by selection on MMP-14 during competition with nTIMP-2, a native inhibitor of MMP-14 binding strongly to its catalytic cleft. 3A2 variants with high potency, selectivity, and improved affinity and proteolytic stability were isolated from a random mutagenesis library. Binding kinetics indicated that the affinity improvements were mainly from slower dissociation rates. *In vitro* degradation tests suggested the isolated variants had half-lives 6–11 fold longer than the wild type. Inhibition kinetics suggested they were competitive inhibitors which showed excellent selectivity toward MMP-14 over highly homologous MMP-9. Alanine scanning revealed that they bound to vicinity of MMP-14 catalytic cleft especially residues F204 and F260, suggesting that the desired epitope was maintained during maturation. When converted to IgG, B3 showed 5.0 nM binding affinity and 6.5 nM inhibition potency with *in vivo* half-life of 4.5 days. In addition to protease inhibitory antibodies, the competitive FACS described here can be applied for discovery and engineering biosimilars, and in general for other circumstances where epitope specific modulation is needed.

TOC

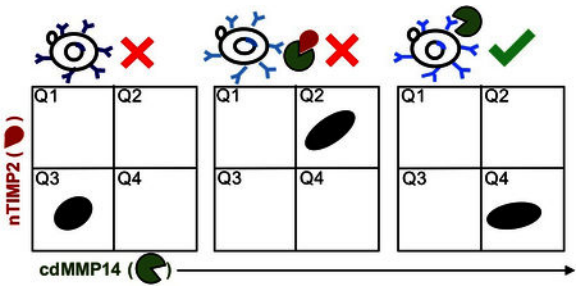

*To whom correspondence should be addressed: Xin Ge, PhD, Associate Professor, Department of Chemical and Environmental Engineering, University of California Riverside, 900 University Ave., Riverside CA 92521 USA, xge@engr.ucr.edu, Phone: 951-827-6229, Fax: 951-827-5696, Website: gelab.ucr.edu.

Epitope specific dual color FACS based on a competitive selection on MMP-14 in the presence of nTIMP-2 was developed to isolate inhibitory antibodies with improved stability and high potency and selectivity

Keywords

epitope specificity; FACS; inhibitory antibody; MMP; proteolytic stability

1. INTRODUCTION

As modulators of molecular interactions with high affinity and high specificity, monoclonal antibodies have emerged as important therapeutics targeting cancers, immune diseases and infections (Buss et al., 2012; Weiner, 2015). In addition to affinity and specificity, the therapeutic efficacy of a given monoclonal antibody often depends on the specific epitope recognized. i.e. exactly where on the antigen binding occurs (Yip et al., 2001; Teeling et al., 2006; Wu et al., 2007; Zhou et al., 2007; He et al., 2016). Since the establishment of hybridoma technology four decades ago, numerous antibody isolation and engineering methods have been developed (Smith, 2015; Chiu, & Gilliland, 2016). The conventional approaches of antibody discovery usually start with binding-based library screening followed by monoclonal characterizations including epitope mapping and function evaluation. Because the later steps are low-throughput and time-consuming, it is desirable to incorporate epitope specificity controls into the initial screening procedures (Puri et al., 2013; Zhang et al., 2006).

One excellent example of epitope specific interaction can be found between proteolytic enzymes and their macromolecular inhibitors (Laskowski & Kato, 1980; Farady, & Craik, 2010; Murphy, 2011). Most protease inhibitory proteins achieve their functions by directly recognizing the protease active site in a substrate-like competitive manner (Nagase et. al. 2006). Inspired by this orthosteric inhibition mechanism, we aimed to develop a high-throughput epitope specific selection method to engineer protease inhibitory antibodies. More specifically, a biomedically important protease, matrix metalloprotease-14 (MMP-14) was chosen as a model target for the development.

MMP-14 is a zinc-dependent endopeptidase associated with tumor growth, metastasis and angiogenesis (Zarrabi et al., 2011; Sela-Passwell et al., 2012; Ager et al., 2015; Remacle et al., 2017). MMP-14 also processes proMMP-2 into active MMP-2, a main contributor to degradation of the extracellular matrix and facilitation of tumor cell migration (Itoh et al., 2001). Previous failures of all broad spectrum MMP small molecule inhibitors in multiple clinical trials taught us that selectivity is key to success of any MMP inhibition therapy (Overall & Kleifeld, 2006). However, the high similarity of protein folding and catalytic chemistry among MMP family members presents a daunting challenge for the generation of highly selective compound inhibitors (Turk, 2006). Our studies (Nam et. al., 2016; Lopez et. al., 2017; Nam et al., 2017), among others (Devy et al., 2009; Udi et al., 2015; Appleby et. al., 2017; Ling et al., 2017), demonstrated the feasibility that antibody based inhibitors could exhibit the desired high selectivity. Particularly, Fab 3A2 with 4.8 nM affinity, 9.7 nM

potency, and high selectivity toward MMP-14 was isolated from a library containing ultra-long CDR-H3s (Nam et. al., 2016). However, like many standard mechanism protease inhibitors or inhibitory mAbs (Farady et al., 2007; Zakharova et al., 2009), 3A2 can be cleaved by its own target, MMP-14, after incubation at low pH for an extended period (Fig S1). For therapeutic development, it is necessary to improve proteolytic stability of 3A2 while retaining its inhibition potency and selectivity.

Cell surface display coupled with fluorescence activated cell sorting (FACS) is a powerful method to select antigen specific antibodies and improve their binding strength and pharmacokinetics (Boder & Witrrup, 2000; Feldhaus et al., 2003; Colby et. al., 2004). During *in vitro* affinity maturation, an existing antibody clone is subjected to site-directed or random mutagenesis (e.g. by error-prone PCR), and generated libraries are displayed on cell surface (e.g. yeast display). After incubation with the fluorescently labelled antigen, cells are quantitatively analyzed for the selection of clones with improved affinity. Notably, affinity maturation can result in epitope drift (Ohlin et al., 1996). For protease-inhibiting antibodies, isolated variants with higher affinities are not necessarily associated with improved inhibition potency. It is possible that through conventional affinity maturation, the epitope can migrate to a region which interferes less with the catalytic pocket, resulting in a reduced inhibition potency. By conjugating MMP-14 and its native inhibitor TIMP-2 with different fluorescent dyes, we have demonstrated that dual color FACS can distinguish inhibitory clones from non-inhibitory clones (Nam et al., 2017). This study further develops this method to improve the proteolytic stability of 3A2, while avoiding unwanted epitope drift and retaining inhibition potency. We test the feasibility to govern control over the epitope by selection on MMP-14 under competition with nTIMP-2. In principle, only the 3A2 variants competing with TIMP-2 binding to inhibitory epitopes, designated MMP-14^{high} and TIMP-2^{low}, will be selected (Fig 1). Furthermore, the *in vitro* and quantitative nature of FACS means that the incubation conditions and sorting windows can be adjusted in real-time to provide high stringency, especially by (1) extending incubation time with MMP-14 and (2) reducing MMP-14 concentration and increasing TIMP-2 concentration, to isolate highly potent inhibitory clones with improved proteolytic resistance.

2. MATERIALS AND METHODS

2.1 Library construction.

Genes of variable heavy (V_H) and variable light (V_L) domains of antibody 3A2 (Nam, et. al. 2016) were amplified to assemble 3A2 scFv (V_H-SGGSGGGGSGSGS-V_L) by overlapping PCR. Error-prone PCR of 3A2 scFv gene was performed by using Taq DNA polymerase with 120 μM dATP, 100 μM dCTP, 360 μM dGTP, 2.5 mM dTTP, 5 μg/mL BSA, 3.28 mM $MgCl_2$ and 0.5 mM $MnCl_2$. The generated mutagenesis product was cloned into the yeast display plasmid pCTcon2 (Feldhaus et al., 2003) by transforming 5 μg ligated DNA into *E. coli* competent cells. 100 μg of library plasmid DNA was used to chemically transform *S. cerevisiae* EBY100 competent cells prepared by Frozen-EZ kit (Zymo). Transformants were selected on SD/-Trp/-Ura (Sunrise Science) agar plates, then collected and stored at −80 °C. Library quality and the mutation rate was analyzed by DNA sequencing of randomly picked clones. For surface display, 5×10^9 library cells were cultured on SD/-Trp/-Ura/penicillin-

streptomycin agar plates at 30 °C for 48 h. 30 OD_{600} of cultured cells were inoculated to 600 mL SD/-Trp/-Ura for incubation at 30 °C, 250 rpm for 12 h. Cells were collected by centrifugation at 6,000 × g for 2 min, and 8 OD_{600} cells were further cultured for scFv expression in 20 mL YNB (yeast nitrogen base)/-Trp/-Ura supplemented with 5 mL 20% galactose at room temperature 250 rpm for 48 h.

2.2 Fluorescent labeling and FACS.

The catalytic domain of MMP-14 was fused with superfolder GFP (Pédelacq et al., 2006), expressed in the periplasm of *E. coli*, and purified with Ni-NTA agarose (Qiagen). Enzymatic activity of the resultant cdMMP14-sfGFP was tested with the FRET peptide substrate, M2350 (Bachem). The N-terminal domain of TIMP-2 (nTIMP-2) was prepared as previously described (Lee et al., 2017), and chemically conjugated with Alexa-647 (Invitrogen). Cells covering 10× the library diversity were sequentially incubated with cdMMP14-sfGFP and nTIMP2-Alexa647 at concentrations adjusted during subsequent rounds of FACS. All incubation steps were performed at RT in the dark for 1 h, and cells were washed with assay buffer (50 mM Tris-HCl pH 7.5, 150 mM NaCl, 5 mM $CaCl_2$, 0.1 mM $ZnCl_2$) between incubations. Cells were sorted on a Bio-Rad S3e flow cytometer equipped with 488/640 nm dual lasers. FL1 (526/48 nm) and FL3 (615/25 nm) were used for GFP and Alexa647 channels respectively. Forward and side scatter voltages were set at 317v and 341v with a threshold of 5. Both scanning and sorting were performed at a rate of 3,000 events/sec with a mild agitation to prevent cell settling. A triangle gate was designed to select cdMMP-14^{high} nTIMP-2^{low} clones. Isolated cells were grown on SD/-Trp/-Ura/ penicillin-streptomycin agar plates at 30 °C for 48 h, and collected in 20% glycerol SD/-Trp/-Ura for storage at −80 °C.

2.3 Antibody production and stability test.

Antibody display plasmids were extracted from isolated yeast clones using a Zymoprep plasmid kit (Zymo) and transformed into *E. coli* for DNA amplification and sequencing. Isolated scFv genes were then cloned into the periplasmic expression vector, pMopac16 (Hayhursta et. al., 2003) for scFvs production. For *in vitro* stability tests, 1 μM purified scFvs were incubated with 1 μM cdMMP-14 in assay buffer at 37 °C for 1–10 h. Densitometric analysis of scFv bands on SDS-PAGE was performed using Image Lab (Bio-Rad). To reduce errors from variations in staining and destaining, gel background for each band was quantified and subtracted. scFv amounts over time were plotted for half-life determination. To produce IgG B3 for *in vivo* stability tests, its V_H and V_L genes were amplified by PCR, and separately cloned to pcDNA-intron-SPL-CH-WPRE and pcDNA-intron-SPL-CL-WPRE plasmids carrying human IgG1 constant heavy and kappa constant light domains with associated signal peptides and Woodchuck hepatitis virus posttranscriptional regulatory elements to enhance the expression (Zufferey et al., 1999). The two plasmids were co-transfected at a ratio of 1:1 into HEK293F cells (3.0×10^6 cells/mL with viability > 98%) with a DNA/PEI “Max” (MW 40,000, Polysciences) mixture at concentrations of 1 μg/mL DNA and 3 μg/mL PEI. The transfected cells were cultured in round bottles at 135 rpm 37°C 8% CO_2 for 7 days. Culture media were clarified by centrifugation and 0.45 μM microfiltration, and B3 IgG was purified by protein A affinity chromatography (GenScript). The concentration of purified IgG was determined by UV

spectrophotometer (BioTek) and its purity was analyzed by SDS-PAGE. To test *in vivo* stability, a single dosage of 100 μg IgG B3 was injected into three 8-week-old female BALB/c mice via tail vein and its clearance was examined by obtaining 50 μl plasma at various time points (2 h, 3, 6, 9, 12 and 15 days). The disappearance of IgG B3 was determined using a human IgG ELISA kit (Sigma). There was no cross-activity in the assay between mouse IgG, or other non-specific binding compounds of mouse serum. The animal procedures were conducted under UCR IACUC approved protocols.

2.4 Antibody characterizations.

Binding kinetics of produced scFvs towards cdMMP-14 were analyzed by bio-layer interferometry BLItz (ForteBio). Purified cdMMP-14 was modified with EZ-link sulfo-NHS-LC-biotin (Thermo Scientific). Streptavidin biosensors were coated with biotinylated cdMMP-14 for 2 min and incubated in 50 mM HEPES (pH 6.8) to establish baselines. 40–800 nM scFvs were introduced and their association to immobilized cdMMP-14 was monitored for 2 min and then allowed to dissociate in 50 mM HEPES for 2 min. Determined k_{on} and k_{off} were used for K_D value calculation. For FRET inhibition assays, 1 μM purified scFv was serially diluted into assay buffer and incubated with 10 nM cdMMP-14 for 30 min at 4 °C. The enzyme kinetic measurements were started with the addition of 1 μM M2350 and the fluorescence was monitored with excitation and emission wavelengths at 325 and 392 nm using a Synergy2 microplate reader (BioTek) equipped with Gen5 software. Inhibition IC_{50} was determined by the change in V_{max} at different concentrations of scFv, and potency K_I was calculated using the equation: $K_I = IC_{50}/(S/K_m+1)$ (Brandt et. al., 1987). Lineweaver-Burk plots were established to determine the type of inhibition. Similarly, purified scFvs were tested against cdMMP-9 and cdMMP-14 single point mutants (Nam et. al., 2016) to determine binding specificity and epitope.

3. RESULTS

3.1 *In vitro* stability of scFv 3A2 wt and mutagenesis library construction.

3A2 was converted to its scFv format (V_H-GS linker-V_L) for yeast surface display. The typical yield of purified scFv 3A2 was 2.5 mg per liter of *E. coli* culture. Toward catalytic domain of MMP-14 (cdMMP-14), scFv 3A2 showed a binding affinity K_D of 25 nM (k_{on} = 1.9×10^5 $M^{-1}s^{-1}$ and k_{off} = 4.9×10^{-3} s^{-1}) and an inhibition potency K_I of 39 nM. When 1 μM scFv 3A2 was incubated with 1 μM cdMMP-14 at 37 °C pH 7.5, scFv 3A2 was quickly degraded to generate fragments at 15 and 16 kDa as the cleavage products. SDS-PAGE analysis of remaining scFv 3A2 samples after incubation with cdMMP-14 for different times indicated a half-life of 1.0 hour (Fig S1). To improve proteolytic stability, scFv 3A2 wt gene was subjected to error-prone PCR, a well-documented and effective random mutagenesis method for antibody engineering (Gram et al., 1992; Daugherty et al., 2000). The generated error-prone product was cloned to the yeast surface display vector carrying an A-agglutinin-binding subunit (aga2), and 4.5×10^8 *E. coli* colonies were obtained. DNA sequencing results of 20 randomly picked clones indicated that mutations occurred across the entire scFv genes with an average mutation rate of 2%, consistent with the experimental design. Transforming library plasmids into *S. cerevisiae* EBY100 resulted in 2×10^7 transformants, which were cultured and induced with 4% galactose for scFv expression. Labeling yeast cells expressing

wt 3A2 scFv with cdMMP14-sfGFP demonstrated that 87% of the population showed a positive signal, while only 0.1% of the non-expressing cells were positive, indicating a successful surface display (Fig S2).

3.2 Epitope specific FACS design and results.

Crystal structure of cdMMP-14 complexed with its native inhibitor nTIMP-2 reveals that the reactive cleft of MMP-14 is directly occupied with a loop conformation of nTIMP-2, formed by its N-terminal residues (Cys1-Val4) and a surface loop (Ala68-Cys72) through a disulfide-bridge between Cys1 and Cys72 (Fernandez-Catalan et al., 1998). Possession of such a substrate-like inhibition mechanism implies that an epitope-specific selection can be achieved by performing a competitive selection on cdMMP-14 in the presence of nTIMP-2. This allows the isolation of inhibitory scFv clones that compete with nTIMP-2 binding to cdMMP-14. In contrast, non-inhibitory scFv clones that bind to epitopes other than the reactive cleft do not compete with nTIMP-2. This results in double positive on both cdMMP-14 and nTIMP-2 signals, and is thus distinguishable from inhibitory clones (Fig 1). To achieve the competitive selection, two fluorophores with different excitation/emission wavelengths were used: cdMMP-14 was fused with superfolder GFP (Pédelacq et al., 2006) and nTIMP-2 was chemically conjugated with Alexa-647. After purification, their functions were confirmed by enzymatic assays using a FRET peptide substrate.

To improve the proteolytic stability, library cells displaying 3A2 mutants were reacted with cdMMP-14 to remove the truncated and thus nonfunctional clones. More specifically, in the first round of sorting, scFv library cells were incubated with 850 nM cdMMP14-sfGFP for one hour, washed, then followed by a competitive interaction with 450 nM nTIMP2-Alexa647. On FACS, 30 million library cells were sorted, and a triangle gate was designed to select the top 1.0 % (3×10^5 cells) of cdMMP14-sfGFP positive cells while excluding the cells with a high nTIMP2-Alexa647 signal (Fig 2). To isolate scFv clones with improved binding affinity and/or inhibition potency, both selection stringency and competition pressure were intensified by decreasing the cdMMP14-sfGFP concentration to 420 nM and 100 nM while increasing nTIMP2-Alexa647 concentration to 500 nM and 1 μM in the second and third rounds of sorting, respectively. Under these conditions, 20 million cells were sorted in R2/R3, and the selection gates were also tightened to the top 0.1% and 0.025% of cdMMP14-sfGFP^{high} and nTIMP2-Alexa647^{low} population, resulting in collection of 2×10^4 and 5×10^3 cells in R2 and R3. When stained with 500 nM cdMMP14-sfGFP and 500 nM nTIMP2-Alexa647, FACS data showed that the proportion of cells in quadrant Q4 (MMP-14^{high} nTIMP-2^{low} cells), was enriched from 2.1% in the original library, to 13.2% in R1, 14.7% in R2 and 20.5% in R3 (Fig 2).

3.3 Monoclonal screening and identifying affinity improved mutants.

Thirty scFv clones randomly picked from R3 were analyzed by monoclonal FACS. Results indicated that the majority (23/30) of isolated mutants had a significantly higher Q4 proportion than 3A2 wt. From this pool of candidates, DNA sequencing the top 10 clones with the highest Q4 % values identified 5 unique clones B1, B3 (6 repeats), T1, T3 and T4, with 4–7 mutations each scattered throughout their scFv genes in both framework regions and CDRs (Table 1). Monoclonal FACS confirmed that Q4 proportions of these mutants

were 12, 15, 24, 23 and 30% respectively, higher than that of 3A2 wt at 10% (Fig S3). Notably, considerable portions of sampled cells (7–15 %) were located at the Q2 quadrant (double positive on both cdMMP14-sfGFP and nTIMP2-Alexa647). FACS analysis of cells after single-labeled with 500 nM nTIMP2-Alexa647 revealed the relatively high backgrounds of non-specific binding of nTIMP2-Alexa647 to yeast cells (Fig S2), explaining the disparity from conceptual populations located at the Q2 quadrant (Fig 1).

The isolated scFv mutant genes were cloned downstream of a pLac promoter and a pelB leader peptide for periplasmic expression in *E. coli* (Hayhurst et al., 2003). Binding kinetics of purified 3A2 mutants on cdMMP-14 were measured by bio-layer interferometry, and results indicated that B1, B3 and T1 exhibited single-digit nanomolar affinities at 4.9, 6.3 and 2.5 nM respectively, significantly stronger than that of 3A2 wt at 25 nM. These improvements were mainly contributed by slower dissociation rates (Table 2), e.g. T1 had a k_{off} of 4.9×10^{-4} s^{-1}, 10-fold slower than that of 3A2 wt ($k_{off} = 4.9\times10^{-3}$ s^{-1}). Affinities of T3 and T4 at 39 and 75 nM were weaker than that of 3A2 wt, which were merely caused by their lower association rates k_{on}s. In fact, k_{off}s of T1 and T3 were improved compared to that of 3A2 wt. Collectively, these results suggested that random mutagenesis followed by dual color epitope-specific FACS generated 3A2 variants with improved affinities especially on disassociation rates k_{off}s, a phenomenon also found by other affinity maturation studies (Yang et al., 1995; Rajpal et al., 2005).

3.4 Isolated 3A2 mutants were MMP-14 inhibitors with high selectivity and improved stability.

Inhibition assays using a FRET peptide substrate indicated that each of the five isolated 3A2 mutants inhibited cdMMP-14 activity, yet with various potencies ranging from 41 nM to 1.3 μM (Table 2). Particularly, B3 and T1 showed their potencies to be less than 100 nM, marginally weaker than that of 3A2 wt (Fig 3A). To demonstrate the selectivity of isolated variants, 1 μM scFvs were incubated with either 10 nM cdMMP-14 or 10 nM highly homologous cdMMP-9 for FRET inhibition assays. Under these conditions, B1, B3 and T1 completely (96–98%) inhibited MMP-14 (Fig 3B), while T4 displayed incomplete inhibition (34%) on MMP-14 due to its low potency (Fig 3A), but none showed cross reactivity on MMP-9 (0% inhibition). However, T3 gave incomplete inhibition on both MMP-14 (70%) and MMP-9 (30%). Therefore, except for T3, other isolated 3A2 mutants exhibited excellent selectivity, similar to 3A2 wt (96% on MMP-14 and 0% on MMP-9). During the *in vitro* stability tests, 1 μM purified scFvs were incubated with 1 μM cdMMP-14 at pH 7.5 37 °C, and samples collected at 1–10 h were densitometrically analyzed for quantification of intact scFvs. As the degradation progress of B3 was shown in Fig S4A, the relative quantities of remaining scFv over time were plotted to determine that the half-life of B3 scFv as 7.5 hours (Fig S4B). Similarly, the half-lives of other isolated 3A2 scFv variants were measured to be 6.2–11.0 hours (Fig 3C, Table 2), significantly longer than 3A2 wt scFv at 1.0 hour (Fig S1). This dramatic improvement in stability was likely achieved by the extended incubation with cdMMP-14 prior to and during FACS experiments, while the inhibition function and selectivity were well retained by controlling the epitope specificity via competition with nTIMP-2 during dual color sorting.

3.5 Isolated 3A2 mutants were competitive inhibitors binding in the vicinity of reactive cleft.

To understand the inhibition mechanism of isolated 3A2 mutants, their inhibitor type was determined by measuring the kinetics of 10 nM cdMMP-14 in the presence of 0, 250, 500, or 1000 nM scFvs. The generated Lineweaver-Burk plots indicated unchanged V_{max}s and increased K_ms with increasing concentrations of scFv (Fig 4, Fig S5), suggesting that all isolated mutants had a competitive mode of inhibition. To further investigate whether these competitive inhibitions were governed by orthosteric or allosteric regulations, we performed alanine scanning on three phenylalanine residues F198, F204 and F260 of cdMMP-14 (Fig 5A). They were chosen because these surface-exposed residues are located around the catalytic cleft (yellow in Fig 5A) and among the binding epitope of nTIMP-2 (red in Fig 5A). cdMMP-14 site-directed mutants F198A, F204A and F260A were produced and incubated with scFvs before their kinetic assays, to check whether these alanine mutations affected the inhibition function of scFvs (Fig 5B). With cdMMP-14 mutant F260A, scFvs T1, T4 and 3A2 wt had no inhibition capability, suggesting that these scFvs interacted with cdMMP-14 wt strongly through F260. However, this was not true of scFvs B1, B3 and T3. In contrast, B1, B3 and T3 showed reduced inhibition of cdMMP-14 mutant F204A to varying degrees, implying that their epitopes at least partially shifted from F260 to F204. Interestingly, clone T1 also showed a reduction in inhibition with the F204A mutant, suggesting that it bound to both F204 and F260, which are located at the two sides of the catalytic center. With F198A, none of the tested scFv clones showed reduced inhibition, indicating tested scFvs did not directly interact with F198. Collectively, the enzyme kinetics and alanine scanning results suggested that isolated 3A2 variants were competitive inhibitors directly binding in the vicinity of the MMP-14 catalytic cleft. Therefore, dual color sorting with nTIMP-2 as the competitor is an effective method to control epitope specificity of isolated antibodies.

3.6 IgG B3 showed nanomolar affinity and potency with expected *in vivo* half-life in mice.

The most promising variant, B3, was converted to its human IgG1 format and produced in HEK293F cells with a typical yield of 35 mg purified IgG per liter of culture media. Binding kinetics of IgG B3 measured by bio-layer interferometry indicated k_{on} of 1.4×10^5 $M^{-1}s^{-1}$ and k_{off} of 7.1×10^{-4} s^{-1} with K_D equal to 5.0 nM (Fig 6A). FRET assays suggested IgG B3 had a similar inhibition potency K_I equal to 6.5 nM (Fig 6B). The *in vivo* clearance rate of IgG B3 in three mice was examined following a bolus injection via tail vein. The amount of IgG B3 present in blood 2 hours after injection was considered the initial circulating concentration (100%). The relative amounts of IgG B3 dropped to 73.1%, 24.2%, 3.6%, 2% and 0.05% at days 3, 6, 9, 12 and 15, respectively (Fig 6C), giving a half-life of ~4.6 days, similar to that of serum immunoglobulins in adult mice (Vieira & Rajewsky, 1988).

4. DISCUSSION:

Studies of therapeutic mAbs have shown that targeting effectual epitopes is absolutely required to produce the desired biological effect. For instance, HIV broadly neutralizing mAb b12 achieves its protective efficacy by recognizing a hidden, but highly conserved, epitope that overlaps with the CD4 binding site on gp120 (Zhou et al., 2007). In the case of

trastuzumab, it binds to domain IV of HER2 extracellular segment, which blocks its signal transduction and inhibits cancer cell growth. However, some HER2-specific mAbs targeting different epitopes exhibit adverse effects by stimulating tumor growth (Yip et al., 2001). To achieve epitope-specific selection, competitive phage panning and FACS have been developed (Puri et al., 2013; Zhang et al., 2006). In an effort to isolate MMP-14 inhibitory mAbs, the use of nTIMP-2, a native inhibitor of MMP-14 as a competitive eluent led to the successful discovery of a panel of inhibitory clones (Devy et al., 2009; Nam et al., 2016). The current study developed a dual color FACS to perform selection on cdMMP-14 under competition with nTIMP-2 to govern needed control over epitope. Furthermore, the quantitative nature of FACS allowed the conditions and sorting windows to be readily adjusted, e.g. by reducing MMP-14 concentration and increasing nTIMP-2 concentration (Fig 2), that provided the desired stringency to generate highly potent inhibitory clones. Using these approaches, we isolated 3A2 variants that exhibited affinity improvement while maintaining high inhibition potency and high selectivity (Table 2 & Fig 3). Our results indicate that even though epitope drift indeed happened for some of isolated clones (e.g. F260 to F204 for scFvs B1 and B3, Fig 5B), dual color competitive FACS kept the effectual epitopes.

Standard mechanism protease inhibitors bind their targets in a substrate-like manner by inserting a reactive loop into the catalytic cleft (Laskowski & Kato, 1980; Farady & Craik, 2010). Upon binding, the scissile bond of the inhibitor is slowly hydrolyzed by the targeted protease (Farady et al., 2007; Zakharova et al., 2009). Improving proteolytic resistance of a protease inhibitor essentially biases toward inhibition rather than substrate behavior. The challenge of such a task was well demonstrated by attempts to generate pepsin/chymotrypsin-resistant hirudin, a thrombin-specific inhibitor. The 5 N-terminal residues and the P1-P1’ positons of major cleavage sites were subjected to mutagenesis. By phage panning, protease-resistant hirudin variants were isolated, however at the expense of ~100-fold reduction in the potency of thrombin inhibition (Wirsching et al., 2003). To address this challenge, Cohen et al. developed an elegant yeast display and multi-modal library screening approach, and successfully engineered Kunitz protease inhibitor domain (APPI) with enhanced proteolytic stability and improved inhibition properties toward mesotrypsin (Cohen et al., 2009). In the current study, we employed prolonged MMP-14 incubation and epitope-specific FACS, and isolated proteolytically resistant inhibitory antibodies with high potency and selection. Notably, the isolated beneficial variants had mutations located throughout the entire scFv gene (Table 1). This suggests that while binding specificity and affinity are largely given by CDRs, the proteolytic stability is strongly influenced by residues within the framework regions, in agreement with other studies (Salameh et al., 2010).

Isolated mutant B1, B3 and T1 scFvs displayed higher binding affinity than 3A2 wt. However, only B3 exhibited similar inhibition potency compared to 3A2 (Table 2). Ideally, inhibitory mAbs should exhibit both high binding affinity and high inhibition potency at similar strength, which indicates that the binding epitopes effectively contribute to inhibition. If affinity strength (K_D) is much higher than that of potency (K_I), e.g. B1 and T1, it is likely caused by less effective epitope that has little interferes on inhibition. Although B3 scFv showed 4-fold improvement on affinity, when converted to IgG, B3 exhibiting a K_D

of 5.0 nM and K_I of 6.5 nM, did not show improvements compared to 3A2 wt IgG (K_D = 3.8 nM, K_I =3.0 nM). Such compromises introduced by format switch are not uncommon for antibody affinity maturation practices. Recent development on Fab yeast display holds great promise for more effective affinity maturation (Wang et al., 2018).

Protein-protein interactions (PPI) are essential for a wide variety of biological functions (Keskin et al., 2016), and for any PPI, epitope specificity is critical. Targeting desired epitopes and avoiding ineffectual or adverse epitopes is also critical for the successful development of biosimilars or biosuperiors. In addition to protease inhibitory antibodies, the competitive FACS described here can be applied for discovery and engineering of biosimilars, and in general for other circumstances where epitope specific modulation is needed.

Supplementary Material

Refer to Web version on PubMed Central for supplementary material.

ACKNOWLEDGEMENTS

This work was supported by the National Institutes of Health 1R01GM115672 and National Science Foundation Faculty Early Career Development Program 1453645.

Grants numbers:

National Institutes of Health 1R01GM115672

National Science Foundation 1453645

REFERENCES

Ager EI, Kozin SV, Kirkpatrick ND, Seano G, Kodack DP, Askoxylakis V, Huang Y, Goel S, Snuderl M, Muzikansky A, Finkelstein DM, Dransfield DT, Devy L, Boucher Y, Fukumura D, & Jain RK (2015). Blockade of MMP14 activity in murine breast carcinomas: implications for macrophages, vessels, and radiotherapy. Journal of National Cancer Institute, 107, djv017.

Appleby T, Greenstein AE, Hung M, Liclican A, Velasquez M, Villaseñor AG, Wang R, Wong MH, Liu X, Papalia GA, Schultz BE, Sakowicz R, Smith V, & Kwon HJ (2017). Biochemical characterization and structure determination of a potent, selective antibody inhibitor of human MMP9. Journal of Biological Chemistry, 292(16), 6810–6820. [PubMed: 28235803]

Boder E & Witrrup KD (2000). Yeast surface display for directed evolution of protein expression, affinity, and stability. Methods in Enzymology, 328, 430–444. [PubMed: 11075358]

Brandt RB, Laux JE, & Yates SW (1987). Calculation of inhibitor K_i and inhibitor type from the concentration of inhibitor for 50% inhibition for Michaelis-Menten enzymes. Biochemical Medicine and Metabolic Biology, 37(3), 344–349. [PubMed: 3606895]

Buss NA, Henderson SJ, McFarlane M, Shenton JM, & de Haan L (2012) Monoclonal antibody therapeutics: history and future. Current Opinion Pharmacology, 12(5), 615–622.

Chiu ML, & Gilliland GL (2016). Engineering antibody therapeutics. Current Opinion in Structural Biology, 38, 163–173. [PubMed: 27525816]

Cohen I, Kayode O, Hockla A, Sankaran B, Radisky DC, Radisky ES, & Papo N (2016). Combinatorial protein engineering of proteolytically resistant mesotrypsin inhibitors as candidates for cancer therapy. Biochemical Journal, 473(10), 1329–1341. [PubMed: 26957636]

Colby D, Kellogg B, Graff C, Yeung Y, Swers J, & Wittrup K (2004). Engineering antibody affinity by yeast surface display. Methods in Enzymology, 388 348–358. [PubMed: 15289082]

Daugherty PS, Chen G, Iverson BL, & Georgiou G (2000). Quantitative analysis of the effect of the mutation frequency on the affinity maturation of single chain Fv antibodies. Proceedings of the National Academy of Sciences of the United States of America, 97(5), 2029–2034. [PubMed: 10688877]

Devy L, Huang L, Naa L, Yanamandra N, Pieters H, Frans N, Chang E, Tao Q, Vanhove M, Lejeune A, van Gool R, Sexton DJ, Kuang G, Rank D, Hogan S, Pazmany C, Ma YL, Schoonbroodt S, Nixon AE, Ladner RC, Hoet R, Henderikx P, Tenhoor C, Rabbani SA, Valentino ML, Wood CR, & Dransfield DT (2009) Selective inhibition of matrix metalloproteinase-14 blocks tumor growth, invasion, and angiogenesis. Cancer Research, 69(4),1517–1526. [PubMed: 19208838]

Farady CJ, & Craik CS (2010). Mechanisms of macromolecular protease inhibitors. ChemBioChem, 11(17), 2341–2346. [PubMed: 21053238]

Farady CJ, Sun J, Darragh MR, Miller SM, & Craik CS (2007). The mechanism of inhibition of antibody-based inhibitors of membrane-type serine protease 1 (MT-SP1). Jounral of Molecular Biolology, 369(4), 1041–1051.

Feldhaus MJ, Siegel RW, Opresko LK, Coleman JR, Feldhaus JM, Yeung YA, Cochran JR, Heinzelman P, Colby D, Swers J, Graff C, Wiley HS, & Wittrup KD (2003). Flow-cytometric isolation of human antibodies from a nonimmune Saccharomyces cerevisiae surface display library. Nature Biotechnology, 21(2),163–170.

Fernandez-Catalan C, Bode W, Huber R, Turk D, Calvete JJ, Lichte A, Tschesche H, & Maskos K (1998). Crystal structure of the complex formed by the membrane type 1-matrix metalloproteinase with the tissue inhibitor of metalloproteinases-2, the soluble progelatinase A receptor. EMBO Journal, 17(17), 5238–5248. [PubMed: 9724659]

Gram H, Marconi LA, Barbas CF, 3rd, Collet TA, Lerner RA, & Kang AS (1992). *In vitro* selection and affinity maturation of antibodies from a naive combinatorial immunoglobulin library. Proceedings of the National Academy of Sciences of the United States of America, 89(8), 3576–3580. [PubMed: 1565653]

Hayhurst A, Happe S, Mabry R, Koch Z, Iverson BL, & Georgiou G (2003). Isolation and expression of recombinant antibody fragments to the biological warfare pathogen *Brucella melitensis*. Journal of Immunological Methods, 276(1–2), 185–196. [PubMed: 12738372]

He W, Tan GS, Mullarkey CE, Lee AJ, Lam MM, Krammer F, Henry C, Wilson PC, Ashkar AA, Palese P, & Miller MS (2016). Epitope specificity plays a critical role in regulating antibody-dependent cell-mediated cytotoxicity against influenza A virus. Proceedings of the National Academy of Sciences of the United States of America, 113(42), 11931–11936. [PubMed: 27698132]

Itoh Y, Takamura A, Ito N, Maru Y, Sato H, Suenaga N, Aoki T, & Seiki M (2001). Homophilic complex formation of MT1-MMP facilitates proMMP-2 activation on the cell surface and promotes tumor cell invasion. EMBO Journal, 20(17), 4782–4793. [PubMed: 11532942]

Keskin O, Tuncbag N, & Gursoy A (2016). Predicting protein-protein interactions from the molecular to the proteome level. Chemical Review, 116(8), 4884–909.

Laskowski M, Jr., & Kato I (1980). Protein inhibitors of proteinases. Annual Review of Biochemistry, 49, 593–626.

Lee KB, Nam DH, Nuhn JA, Wang J, Schneider IC, & Ge X (2017). Direct expression of active human tissue inhibitors of metalloproteinases by periplasmic secretion in Escherichia coli. Microbial Cell Factory, 16, 73.

Ling B, Watt K, Banerjee S, Newsted D, Truesdell P, Adams J, Sidhu SS, & Craig AWB (2017). A novel immunotherapy targeting MMP-14 limits hypoxia, immune suppression and metastasis in triple-negative breast cancer models. Oncotarget, 8(35), 58372–58385. [PubMed: 28938563]

Lopez T, Nam DH, Kaihara E, Mustafa Z, & Ge X (2017). Identification of highly selective mmp-14 inhibitory fabs by deep sequencing. Biotechnology and Bioengineering, 114(6), 1140–1150. [PubMed: 28090632]

Murphy G (2011). Tissue inhibitors of metalloproteinases. Genome Biology, 12, 233. [PubMed: 22078297]

Nagase H, Visse R, & Murphy G (2006). Structure and function of matrix metalloproteinases and TIMPs. Cardiovascular Research, 69, 562–573. [PubMed: 16405877]

Nam DH, Fang K, Rodriguez C, Lopez T, & Ge X (2017). Generation of inhibitory monoclonal antibodies targeting matrix metalloproteinase-14 by motif grafting and CDR optimization. Protein Engineering, Design & Selection, 30(2), 113–118.

Nam DH, Rodriguez C, Remacle AG, Strongin AY, & Ge X (2016). Active-site MMP-selective antibody inhibitors discovered from convex paratope synthetic libraries. Proceedings of the National Academy of Sciences of the United States of America, 113(52), 14970–14975. [PubMed: 27965386]

Ohlin M, Owman H, Mach M, & Borrebaeck CA (1996). Light chain shuffling of a high affinity antibody results in a drift in epitope recognition. Molecular Immunology, 33(1), 47–56. [PubMed: 8604223]

Overall CM, & Kleifeld O (2006). Towards third generation matrix metalloproteinase inhibitors for cancer therapy. British Jounral of Cancer, 94(7), 941–946.

Pédelacq JD, Cabantous S, Tran T, Terwilliger TC, & Waldo GS (2006). Engineering and characterization of a superfolder green fluorescent protein. Nature Biotechnology, 24(1),79–88.

Puri V, Streaker E, Prabakaran P, Zhu Z, & Dimitrov DS (2013). Highly efficient selection of epitope specific antibody through competitive yeast display library sorting. mAbs, 5(4), 533–539. [PubMed: 23765162]

Rajpal A, Beyaz N, Haber L, Cappuccilli G, Yee H, Bhatt RR, Takeuchi T, Lerner RA, & Crea R (2005). A general method for greatly improving the affinity of antibodies by using combinatorial libraries. Proceedings of the National Academy of Sciences of the United States of America, 102(24), 8466–8471. [PubMed: 15939870]

Remacle AG, Cieplak P, Nam DH, Shiryaev SA, Ge X, & Strongin AY (2017). Selective function-blocking monoclonal human antibody highlights the important role of membrane type-1 matrix metalloproteinase (MT1-MMP) in metastasis. Oncotarget, 8(2), 2781–2799. [PubMed: 27835863]

Salameh MA, Soares AS, Navaneetham D, Sinha D, Walsh PN, & Radisky ES (2010). Determinants of affinity and proteolytic stability in interactions of Kunitz family protease inhibitors with mesotrypsin. Journal of Biological Chemistry, 285(47), 36884–36896. [PubMed: 20861008]

Sela-Passwell NA, Kikkeri R, Dym O, Rozenberg H, Margalit R, Arad-Yellin R, Eisenstein M, Brenner O, Shoham T, Danon T, Shanzer A, & Sagi I (2012). Antibodies targeting the catalytic zinc complex of activated matrix metalloproteinases show therapeutic potential. Nature Medcine, 18(1), 143–147.

Smith AJ. New Horizons in Therapeutic antibody discovery: opportunities and challenges versus small-molecule therapeutics. Journal of Biomolecular Screening. 2015 20(4), 437–453. [PubMed: 25512329]

Teeling JL, Mackus WJ, Wiegman LJ, van den Brakel JH, Beers SA, French RR, van Meerten T, Ebeling S, Vink T, Slootstra JW, Parren PW, Glennie MJ, & van de Winkel JG (2006). The biological activity of human CD20 monoclonal antibodies is linked to unique epitopes on CD20. Journal of Immunology, 177, 362–371.

Turk B (2006). Targeting proteases: successes, failures and future prospects. Nature Review Drug Discovery, 5(9), 785–799. [PubMed: 16955069]

Udi Y, Grossman M, Solomonov I, Dym O, Rozenberg H, Moreno V, Cuniasse P, Dive V, Arroyo A, & Sagi I (2015). Inhibition mechanism of membrane metalloprotease by an exosite-swiveling conformational antibody. Structure, 23, 104–115. [PubMed: 25482542]

Vieira P, & Rajewsky K (1988). The half-lives of serum immunoglobulins in adult mice. European Journal of Immunology, 18, 313–316. [PubMed: 3350037]

Wang B, DeKosky BJ, Timm MR, Lee J, Normandin E, Misasi J, Kong R, McDaniel JR, Delidakis G, Leigh KE, Niezold T, Choi CW, Viox EG, Fahad A, Cagigi A, Ploquin A, Leung K, Yang ES, Kong WP, Voss WN, Schmidt AG, Moody MA, Ambrozak DR, Henry AR, Laboune F, Ledgerwood JE, Graham BS, Connors M, Douek DC, Sullivan NJ, Ellington AD, Mascola JR, & Georgiou G (2018). Functional interrogation and mining of natively paired human VH:VL antibody repertoires. Nature Biotechnology, 36(2), 152–155.

Weiner GJ (2015) Building better monoclonal antibody-based therapeutics. Nature Review Cancer, 15(6), 361–370. [PubMed: 25998715]

Wirsching F, Keller M, Hildmann C, Riester D, & Schwienhorst A (2003). Directed evolution towards protease-resistant hirudin variants. Molecular Genetics and Metabolism, 80 (4), 451–462. [PubMed: 14654359]

Wu Y, Eigenbrot C, Liang WC, Stawicki S, Shia S, Fan B, Ganesan R, Lipari MT, & Kirchhofer D (2007). Structural insight into distinct mechanisms of protease inhibition by antibodies. Proceedings of the National Academy of Sciences of the United States of America, 104(50), 19784–19789. [PubMed: 18077410]

Yang WP, Green K, Pinz-Sweeney S, Briones AT, Burton DR, & Barbas CF, 3rd. (1995). CDR walking mutagenesis for the affinity maturation of a potent human anti-HIV-1 antibody into the picomolar range. Journal of Molecular Biology, 254(3), 392–403. [PubMed: 7490758]

Yip YL, Smith G, Koch J, Dübel S, & Ward RL (2001). Identification of epitope regions recognized by tumor inhibitory and stimulatory anti-ErbB-2 monoclonal antibodies: implications for vaccine design. Journal of Immunology, 166(8), 5271–5278.

Zakharova E, Horvath MP, & Goldenberg DP (2009). Structure of a serine protease poised to resynthesize a peptide bond. Proceedings of the National Academy of Sciences of the United States of America, 106 (27), 11034–11039. [PubMed: 19549826]

Zarrabi K, Dufour A, Li J, Kuscu C, Pulkoski-Gross A, Zhi J, Hu Y, Sampson N, Zucker S, & Cao J (2011). Inhibition of matrix metalloproteinase 14 (mmp-14)-mediated cancer cell migration. Journal of Biological Chemistry, 286(38), 33167–33177. [PubMed: 21795678]

Zhang MY, Choudhry V, Sidorov IA, Tenev V, Vu BK, Choudhary A, Lu H, Stiegler GM, Katinger HW, Jiang S, Broder CC, & Dimitrov DS (2006). Selection of a novel gp41-specific HIV-1 neutralizing human antibody by competitive antigen panning. Journal of Immunological Methods, 317(1–2), 21–30. [PubMed: 17078964]

Zhou T, Xu L, Dey B, Hessell AJ, Van Ryk D, Xiang SH, Yang X, Zhang MY, Zwick MB, Arthos J, Burton DR, Dimitrov DS, Sodroski J, Wyatt R, Nabel GJ, & Kwong PD (2007). Structural definition of a conserved neutralization epitope on HIV-1 gp120. Nature, 445(7129), 732–737. [PubMed: 17301785]

Zufferey R, Donello JE, Trono D, & Hope TJ (1999). Woodchuck hepatitis virus posttranscriptional regulatory element enhances expression of transgenes delivered by retroviral vectors. Journal of Virology, 73(4), 2886–2892. [PubMed: 10074136]

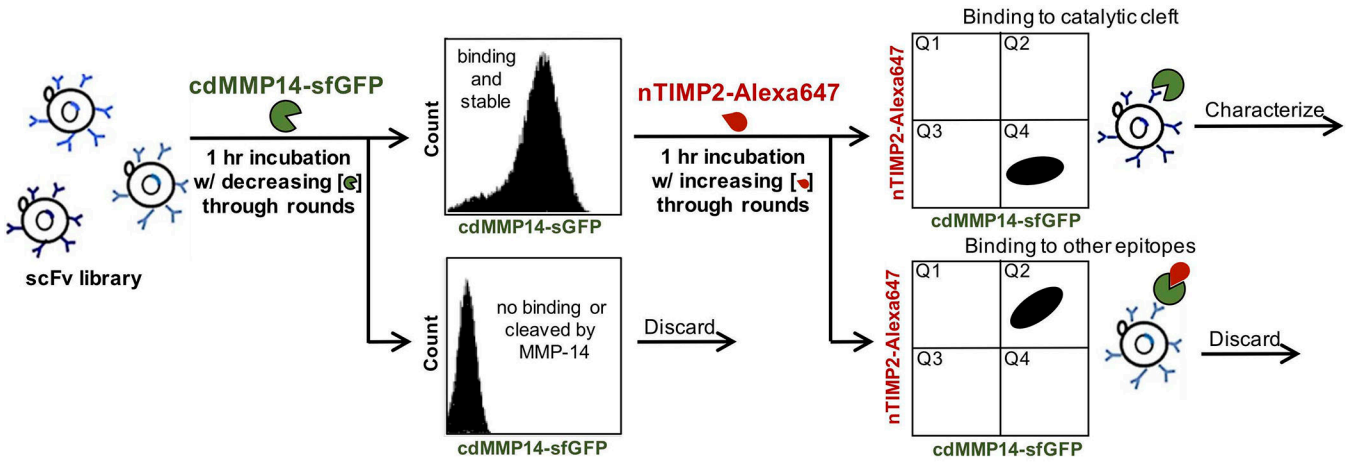

Figure 1.

Scheme of dual color epitope specific FACS for inhibitory antibodies with improved stability and high potency.

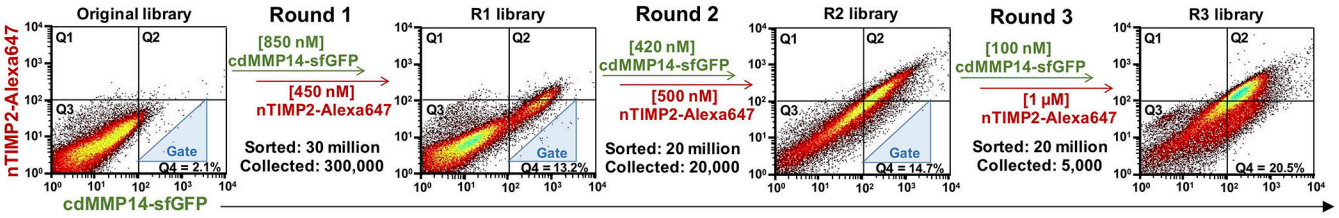

Figure 2.

Progress of three rounds of epitope specific FACS sorting. Concentrations of cdMMP14-sfGFP and nTIMP2-ALEXA647 for each round are indicated. Triangle sorting gates are shown. And proportions of cells in Q4, representing MMP-14^{high} and nTIMP-2^{low} were also calculated.

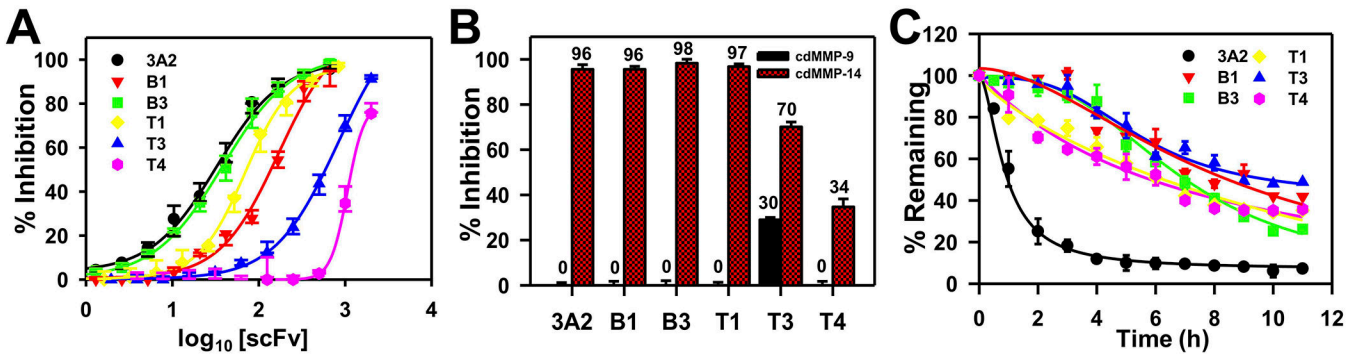

Figure 3.

Characterization of isolated scFv clones. (A) Inhibition assays with 10 nM cdMMP-14, 0–2000 nM scFv and 1 μM FRET peptide substrate. (B) Selectivity on MMP-14 over MMP-9 demonstrated by relative inhibition. (C) *In vitro* stability results. Following 1 μM scFv incubation with 1 μM cdMMP-14 for indicated period time, SDS-PAGE bands associated with intact scFvs were quantitatively analyzed to calculate half-lives. See Figs S1&S4 for examples. Error bars indicate standard deviations from three independent measurements.

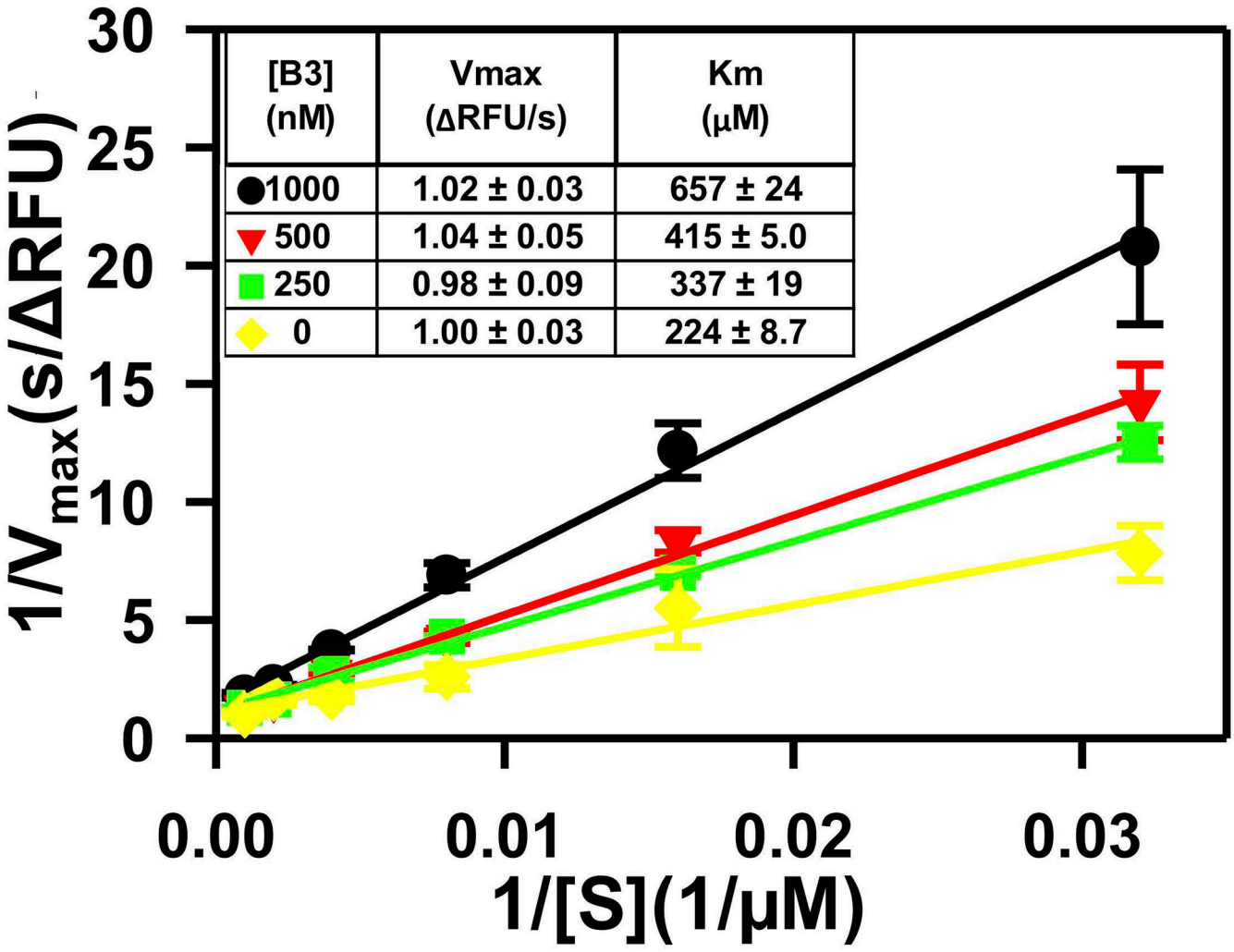

Figure 4.

Determination of inhibition mode of scFv B3. Enzymatic kinetics were measured in the presence of 0, 250, 500 and 1000 nM scFv B3. Lineweaver-Burk plots were generated to calculate V_{max} and K_m. Error bars indicate standard deviations from two independent measurements.

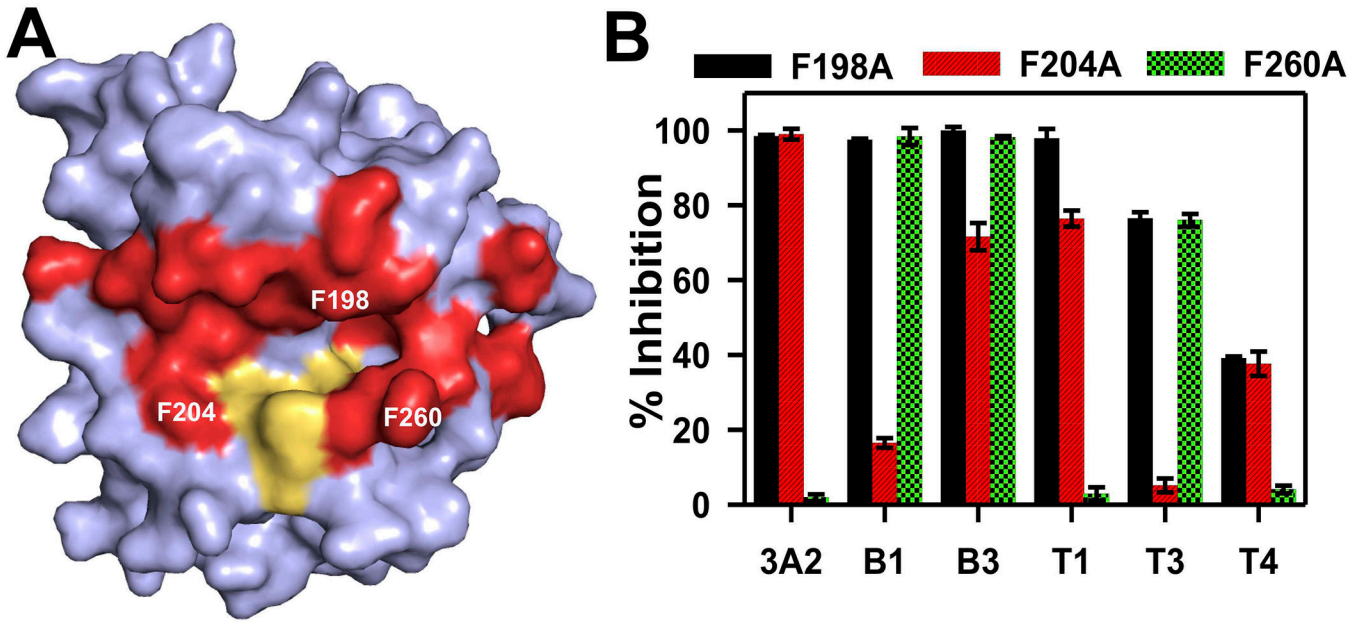

Figure 5.

Epitope mapping of scFvs 3A2 wt and isolated variants. (A) Catalytic domain of MMP14 showing the reaction center (yellow) and binding region of TIMP-2 (red). The three phenylalanine residues selected for single site alanine mutations were labeled. (B) Relative inhibition of scFvs on cdMMP-14 mutants. 10 nM cdMMP-14, 1 μM scFv and 1 μM peptide substrate were used. Error bars indicate standard deviations from three independent measurements.

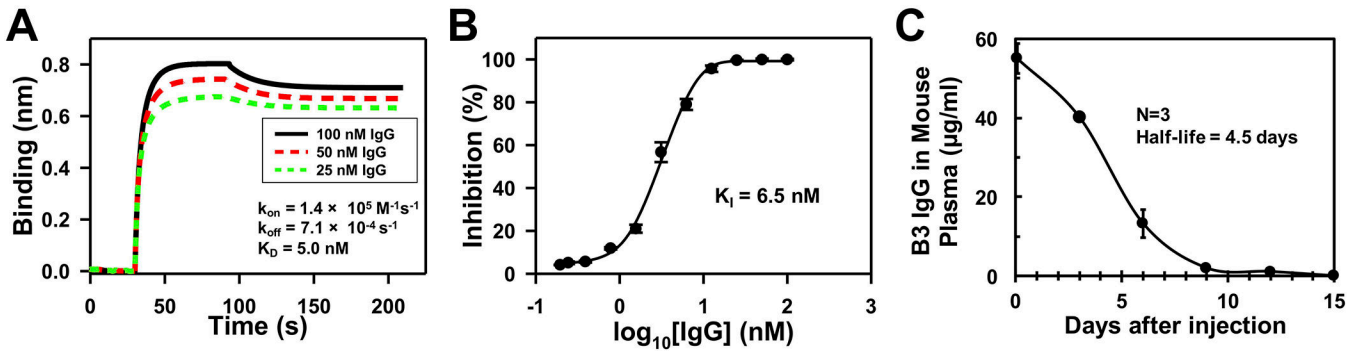

Figure 6.

Characterization of IgG B3. (A) Binding kinetics. (B) Inhibition potency. (C) *In vivo* stability of IgG B3 antibody. N=3 for each time point and data are presented as the mean ± S.D.

Table 1.

scFv clones obtained from monoclonal FACS studies

ScFv	Q4 (%)	Mutations	
		Light Chain	Heavy Chain
3A2	10	-	-
B1	12	M4I; V19A; P94S	Y100nF; G104D; T107S
B3 (6 repeats)	15	A13T; S14T	P14L; V37A; G44D; Y58H; Y102H
T1	24	R18W; F62L; T69M	A40V
T3	23	M4K; C23S; E81K	M100rT
T4	30	D17G; V19S; K39E; T72S	-

Table 2.

Biochemical characterizations of scFv 3A2 wt and isolated variants.

Standard deviations were calculated from three independent measurements.

scFv	k_{on} (1/Ms)	k_{off} (1/s)	K_D (nM)	Potency (nM)	Inhibition type	In vitro half-life (h)
3A2	1.9×10^{5}	4.9×10^{-3}	25 ± 2.1	39 ± 4.2	Competitive	1.0 ± 0.2
B1	7.9×10^{5}	3.9×10^{-3}	4.9 ± 1.7	150 ± 3.5	Competitive	9.0 ± 0.3
B3	3.5×10^{5}	2.2×10^{-3}	6.3 ± 2.4	41 ± 1.9	Competitive	7.5 ± 0.5
T1	2.0×10^{5}	4.9×10^{-4}	2.5 ± 1.3	79 ± 4.1	Competitive	6.8 ± 0.4
T3	6.2×10^{4}	2.4×10^{-3}	39 ± 4.6	572 ± 3.8	Competitive	11.0 ± 0.1
T4	5.3×10^{4}	4.0×10^{-3}	75 ± 3.8	1323 ± 5.3	Competitive	6.2 ± 0.6